A UNIFIED MODEL FOR ION DEPOSITION AND THERMOMECHANICAL RESPONSE IN DRY WALL LASER IFE CHAMBERS

James P. Blanchard[1], Qiyang Hu[2], and Nasr Ghoniem[2]

[1]*University of Wisconsin, Madison, WI, blanchard@engr.wisc.edu*
[2]*University of California, Los Angeles, CA, huqy@seas.ucla.edu, nghoniem@gmail.com*

Dry wall laser IFE chambers will experience large, transient heat and particle fluxes as the target yield products reach the wall. These threats, consisting of x-rays, ions, and neutrons, can lead to wall failure caused by transient stresses or as a result of deposited ions in the near-surface layer. We have developed a unified model for the calculation of temperatures, stresses, strains, and fracture behavior in a solid IFE chamber wall. The model is also coupled with ion transport sub-models that assess the effects of ions on the morphology of the wall materials. This paper describes the models incorporated into the new unified simulation and, in particular, presents new fracture models that permit fracture calculations without the need for an advanced finite element calculation. This fracture model assumes that an array of surface cracks is present in the wall surface and uses superposition to calculate the stress intensity factor via a numerical integration of the stress profile computed for an un-cracked geometry. We also describe approaches for computing the stresses due to inertial effects resulting from the rapid heating associated with the IFE threats. In some cases, these inertial effects lead to stress waves that can lead to premature wall damage and must be accounted for in the analysis. This model is based on semi-analytical solutions for stress waves due to shallow heating in a relatively thick solid. The combined thermomechanical model gives us detailed understanding of the fundamental mechanics of rapidly heated surfaces.

I. INTRODUCTION

In order to permit the design of an economically viable IFE power plant, we require a chamber wall that will survive on the order of 1 billion shots, assuming the chamber operates at a shot frequency of 10 Hz for a few years without requiring wall replacement. On each shot, the wall must withstand a typical target threat, consisting of significant fluxes of x-rays, ions, and neutrons. These threats will cause large temperature excursions at the wall surface, depending on the target yield, the chamber material properties, and the distance from the target to the wall.

There are two primary damage mechanisms of concern to dry-wall IFE chambers. The first is thermomechanical in nature, where the large temperature excursions caused by the threats lead to large stresses and subsequent failure caused by fracture or fatigue cracking. The second damage mechanism is related to the ions, which, after implantation, tend to cluster together, form bubbles, and thus cause dramatic changes to the wall surface. These morphology changes can potentially lead to mass loss and thus are a concern with respect to wall lifetime.

Previous models for these phenomena have been uncoupled, so they were susceptible to inconsistencies that produced uncertainty in the results. To eliminate these inconsistencies, we have constructed a computer code that unifies the existing thermomechanical and ion behavior models into a single simulation. In addition, we have introduced some simplifications in the models in order to produce more rapid results and to facilitate the coupling. In this paper we describe the models incorporated into this computer code and discuss comparisons to other more detailed calculations in order to validate the new, simplified models.

II. DEPOSITION MODELS

The analysis begins with models for x-ray and ion deposition. This is needed to produce heating profiles for the thermal modeling and, in the case of ion effects, we require time-dependent ion deposition profiles. Subsequent diffusion calculations will model the post-deposition ion motion. The x-ray and ion spectra for a typical High Average Power Laser (HAPL) target can be found in Ref. 1.

The x-ray deposition is modeled using energy-dependent attenuation coefficients from NIST (Ref. 2). Ion deposition is more difficult, as the form of the stopping power depends on the ion energy. For the unified code, we have used the SRIM code (Ref. 3) to generate stopping powers as a function of energy in each material of interest. These stopping powers were then fit to the following formula (following Ref. 4, equation 32):

$$S = \frac{A}{\left(\frac{B}{\sqrt{E}} + \frac{CE}{ln(1+DE)}\right)} \quad (1)$$

where S is the stopping power, E is the ion energy, and A, B, C, and D are fitting parameters. This formula is then used to track the ion energy as a function of depth and thus compute ion range as a function of incident energy, as well as the heating vs. depth. Once generated, this formula allows us to model the ion deposition without having to resort to Monte Carlo analysis, thus providing more rapid computation of the heating profile.

III. THERMAL MODELING

To determine the wall temperature distributions, the ion and x-ray heating rates are incorporated into a 1-D conduction model using a finite difference approach. Thermal properties are temperature-dependent and multiple material layers are permitted.

IV. STRESS MODELS

The assumptions of the stress models in this code have been presented earlier (Ref. 5). Since only a thin layer of the chamber wall surface is heated, it is prevented from expanding laterally by the underlying cold material. Hence, the only material displacement allowed is perpendicular to the surface. Hence, the displacement models are one-dimensional with no total strain permitted parallel to the wall surface. For elastic deformation, this leads to a fairly simple formula for the transverse stress in the wall, assuming constant surface heating, and a semi-infinite geometry

$$\sigma_{xx} = \sigma_{xx} = \frac{-E\alpha T}{(1-\upsilon)} \quad (2)$$

where E is the elastic modulus, α is the thermal expansion coefficient, T is the surface temperature change from the stress-free temperature, and υ is the Poisson's ratio. For most cases, we expect plasticity, so we have implemented an incremental plasticity model to permit the calculation of plastic strains for both loading and unloading conditions.

V. FRACTURE MODELS

In many cases, especially for metal walls, the primary failure mode is surface cracking. During a heat pulse, the wall surface is put into compression as the surface is constrained from expansion by the underlying cooler material. The surface thus yields and the stress becomes quite low as the yield stress drops with the increasing temperature. The surface is thus placed in a nearly stress-free condition, due to the very low yield stress at the peak wall temperature. Therefore, as the wall cools, the surface stress becomes tensile as the surface cools from this low-stress state. It is this tensile stress that leads to subsequent cracking. Our fracture model incorporates a superposition approach, where we first calculate the stress profile in an un-cracked geometry using a single loading and unloading cycle. This leads to a tensile stress field after the wall surface cools. We then consider the case of a single surface crack with a point load (F) on the surface of a crack of depth a, as shown in Fig. 1.

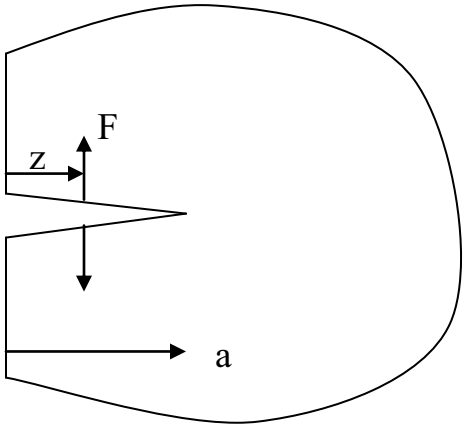

Fig. 1 Geometry for point load on crack surface. This geometry is used to generate a Green's function that can be used to calculate the stress intensity factor for surface cracks in IFE chamber walls.

The stress analysis for an un-cracked geometry will, upon cooling, yield a tensile stress field that can be represented by $\sigma_{xx}(s)$, where s is the dimensionless depth (s=z/a) and a is the crack depth. By superimposing on this solution an appropriate set of forces such as those in Fig. 1, we can effectively create a traction-free surface, thus representing a surface crack. Hence, the stress intensity factor for the cracked geometry becomes

$$K_I = \int_0^1 \sqrt{a}\frac{G(s)}{\sqrt{1-s}}\sigma(s)\,ds \quad (3)$$

where G(s) is the solution to the problem from Fig. 1. This solution is found to be (Ref. 6)

$$G(s) = \sqrt{\frac{2}{\pi}}[1 + 0.6147(1-s) + 0.2502(1-s)^2] \quad (4)$$

To assess the validity of this approach, we analyzed a standard HAPL chamber for 350 MJ target with a 10.5 meter radius chamber. The wall surface is assumed to be tungsten. The stress intensity factor (K_I) is shown as a function of the crack depth in Figs. 2&3. At each time, there exists a crack depth that would maximize the stress intensity factor. Hence, for each step the code calculates the stress intensity for a variety of crack depths and identifies the crack depth corresponding to the maximum. Fig. 2 plots the maximum stress intensity factor as a function of time and the axis on the right plots the crack depth at which that maximum occurs.

As shown in this figure, the stress intensity factor initially increases roughly as the square root of the crack length, as would be expected for a region of constant stress, but asymptotes as the crack length increases further, because the stresses decrease as the crack approaches cooler regions. If the critical K_I is to be 7 MPa·m$^{1/2}$ for recrystalized tungsten (Ref 7), the critical crack length will be reached at 24 μm after 1.2 microseconds.

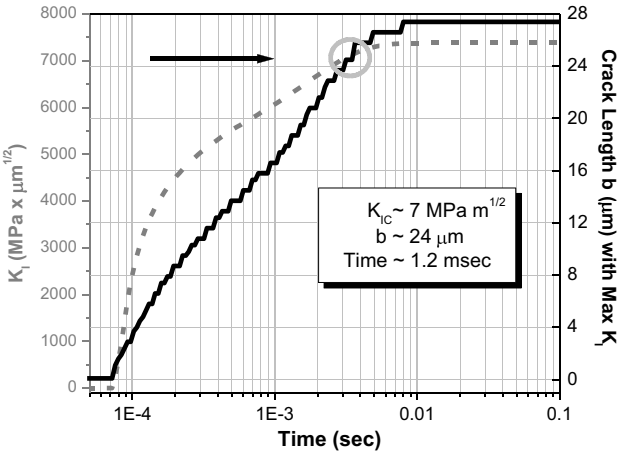

Fig. 2. Maximum stress intensity factor and corresponding crack depth as a function of time for a typical tungsten coated wall.

We can follow a similar approach to consider an array of surface cracks. For this problem, we require a solution for point loads on the surfaces of an array of surface cracks. In this case, we followed Ref. 8, though we believe the results in this paper are in error. Hence, we generated the Green's functions using finite element simulations, but fit them to the form given in Ref. 8. In this case, the Green's function [G(s)] is assumed to be a linear function of s and the slope and intercept of these functions vary with the crack spacing (h). In other words, we have

$$G(s) = ms + t \qquad (5)$$

And these slope and intercept values are given in Table 1.

To assess the validity of this approach for crack arrays, we analyzed a standard HAPL target for tungsten wall containing a periodic array of surface cracks. As can be seen in this figure, a crack spacing that is four times the crack depth reduces the stress intensity factor, relative to that for an isolated crack, by roughly a factor of 2. This explains the crack arrays seen in surface heated tungsten (Ref. 9), as arrays of cracks will tend to relieve stress and lead to crack arrest.

Ratio of h/a	m	t
2	0.6798	0.0128
4	0.1567	0.5795
8	-0.4041	1.1349
12	-0.5670	1.3000
16	-0.6312	1.3640
20	-0.6614	1.3943

Table 1: Slope and intercept values to be used in Equation 5 to generate Green's function for stress intensity factors in an array of surface cracks.

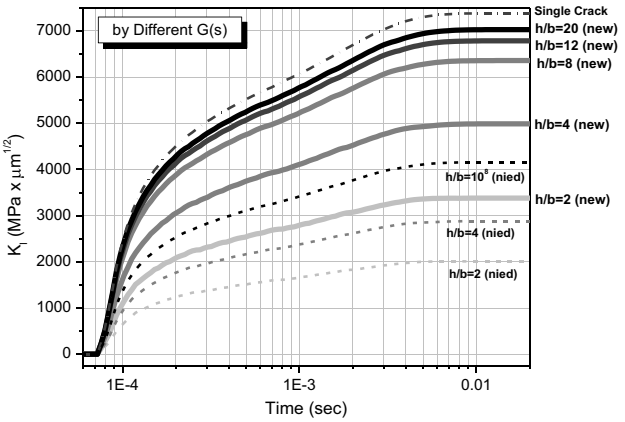

Fig. 3 Stress intensity factor in tungsten wall containing surface crack array as a function of crack depth for different crack spacings. The dotted lines represent the results using the table from Ref. 8. The solid lines are our corrected results, using Eq. 5 and Table 1.

VI. INERTIAL EFFECTS (STRESS WAVES)

Due to the rapid heating associated with IFE targets, stress waves of consequence can be launched in the chamber wall. In many situations, the stresses associated with the waves are small compared to the steady stresses discussed above. However, in some cases, particularly those with the shortest pulse lengths, the inertial stresses are appreciable and must be accounted for in the analysis. Simplified models are available for estimation of these

effects (Ref. 10), but more comprehensive models are needed to assess the effects of the complicated loading histories and deposition profiles associated with an IFE target. Ultimately, the unified model will incorporate a full numerical simulation, but in the interim we have implemented a superposition model based on an analytical model for the stress waves induced by a heating which is applied as a step change in time and has an exponential profile. This is a reasonable approximation for mono-energetic x-rays, but still is limited with respect to the complex heating of an IFE target.

To implement the superposition approach, we model a heating history as a series of step changes in the heating rate. Each of these time steps is associated with an increment of heating and each of these steps launches a small stress wave. We can superimpose a series of these steps to approximate a more complex heating history. For example, if the peak heating rate is ramped, increasing linearly, this can be approximated by a series of steps, as shown in Fig. 4.

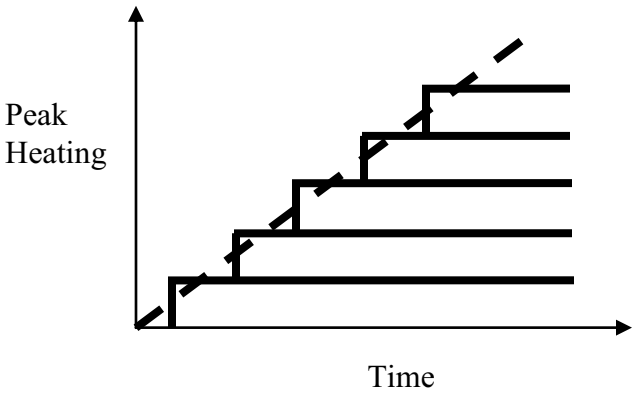

Fig. 4 Comparison of a case of ramped heating (dashed line) to a series of incremental steps. In either case, the plot is of the surface heating and the depth profile is exponential.

The solution used for the step heating increments can be found in Ref. 10.

To test the validity of this approach, the two cases depicted in Fig. 4 were run for parameters that are representative of a typical direct-drive target yield on a tungsten-coated wall. The results are shown in Fig. 5, which demonstrates that the error in the stresses calculated from a superposition from a series of step-heating cases is small, as compared to an exact solution for ramped heating.

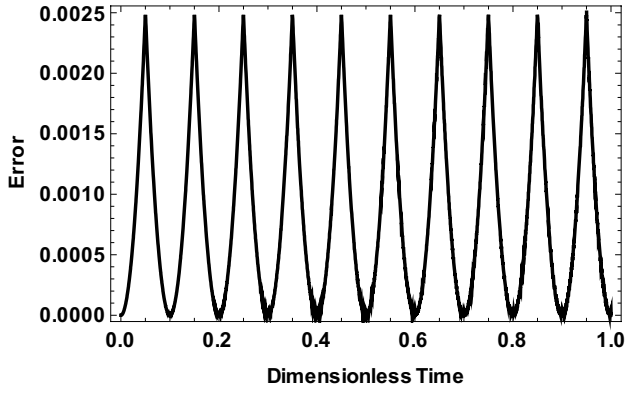

Figure 5 Relative Error between exact and approximate solutions for transverse stress at surface in ramped heating case. The error is normalized to the peak stress and the time is normalized to the pulse length.

VII. ION TRANSPORT MODELS

A numerical code (HEROS), which embodies the spatially-dependent Cluster Dynamic theory, has been developed for the HAPL project in order to permit modeling of ion transport and clustering in IFE chamber walls (Ref 11). It uses a set of 13 master equations to model the evolution of the following 13 species: (1) unoccupied single vacancies; (2) single self-interstitial atoms; (3) interstitial helium atoms; (4) substitutional helium atoms; (5) di-interstitial helium atom clusters; (6) di-helium single vacancy clusters; (7) bubble nuclei (containing 3 helium atoms without a single vacancy); (8) large bubbles containing *m* helium atoms, (9) average matrix-bubble size; (10) average number of helium atoms in a matrix bubble; (11) amount of helium absorbed in grain boundaries (using a single grain boundary density parameter); (12) average precipitate bubble radius; and (13) amount of helium in precipitate bubbles. The spatially homogeneous master rate equations are based on the detailed derivation given in Ref 12. The code has been shown to be capable of modeling space-dependent helium transport in finite geometries, including the simultaneous transient production of defects and space- and time-dependent temperature and temperature gradient fields (Ref 11). Space-dependent nucleation and growth of helium bubbles during implantation are modeled along with the impact of biased migration and coalescence of Helium bubbles.

We are in the process of coupling this code to the thermomechanical models in order to provide a fully-coupled code for simulating the primary failure modes of dry-wall IFE chambers.

VIII. FUTURE WORK

There is work in progress to make a variety of improvements to this unified code for modeling IFE chamber walls. These include

- Conversion of the approximate inertial stress models described here to a full numerical solution of the appropriate wave equation
- Addition of a graphical interface to make it easier for others to use
- Move to a 2-D or 3-D geometry to permit consideration of individual grains and grain boundaries, as well as engineered structures

CONCLUSIONS

We are in the process of developing a series of thermomechanical and helium models suitable for the development of a fully coupled, unified chamber wall model. To this point, suitable models are available for calculating

- Static stresses and strains, including plastic deformation
- Stress intensity factors suitable for predicting crack propagation
- All relevant ion transport and clustering phenomena

Ongoing work is developing models for inertial effects.

ACKNOWLEDGMENTS

The authors would like to thank the High Average Power Laser (HAPL) project for support of this work.

REFERENCES

1. A. R. RAFFRAY and the HAPL Team**,** "Threats, Design Limits and Design Windows for Laser IFE Dry Wall Chambers," J. Nuc. Mat., **347**, 178 (2005).
2. http://physics.nist.gov/PhysRefData/
3. http://www.srim.org/
4. J. P. BIERSACK and L. G. HAGGMARK, "A Monte Carlo Computer Program for the Transport of Energetic Ions in Amorphous Targets," Nuc. Inst. Meth., **174**, 257 (1980).
5. JAMES P. BLANCHARD and CARL J. MARTIN, "Thermomechanical effects in a laser IFE first wall," J Nuc Mat, **347**, 192 (2005)
6. ALTEN F. GRANDT Jr., 229, *Fundamentals of Structural Integrity,* Wiley-IEEE (2004).
7. E.I. USKOV and A.V. BABAK, "Examination of the high-temperature cracking resistance of tungsten." OSTI Ind. Lab, **49**, 852 (1984).
8. H. F. NIED, "Periodic Array of Cracks in a Half-Plane Subjected to Arbitrary Loading," J. Appl. Mech., **54**, 642 (1987).
9. T.J. RENK, P.P. PROVENCIO, T.J. TANAKA, C.L. OLSON, R.R. PETERSON, J.E. STOLP, D.G. SCHROEN and T.R. KNOWLES "Chamber wall materials response to pulsed ions at power-plant level fluencies," **J. Nuc. Mat.,** 347**,** 266 (2005).
10. J. CONZEN and J. BLANCHARD, "An Upper Bound For Stress Waves Induced By Volumetric Heating In IFE Chamber Walls," Fus Sci Tech, **52**, 506 (2007).
11. Q. HU, S. SHARAFAT and N.M. GHONIEM, "Modeling Space-Time Dependent Helium Bubble Evolution in Tungsten Armor Under IFE Conditions," Fus Sci Tech, **52**, 574 (2007)
12. N.M. GHONIEM, J.N. ALHAJJI, and D. KALLETA, *J. Nucl. Mater.* **136**, 192-206 (1985)